ACS Partner Journal

Journal of the American Society for Mass Spectrometry

pubs.acs.org/jasms

Research Article

# Field-Switching Repeller Flowing Atmospheric-Pressure Afterglow Drift Tube Ion Mobility Spectrometry

Mohsen Latif, Xi Chen, Viraj D. Gandhi, Carlos Larriba-Andaluz,* and Gerardo Gamez*

Cite This: https://doi.org/10.1021/jasms.1c00309

Read Online



**ABSTRACT:** In this work, a field-switching (FS) technique is employed with a flowing atmospheric pressure afterglow (FAPA) source in drift tube ion mobility spectrometry (DTIMS). The premise is to incorporate a tip-repeller electrode as a substitute for the Bradbury−Nielsen gate (BNG) so as to overcome corresponding disadvantages of the BNG, including the gate depletion effect (GDE). The DTIMS spectra were optimized in terms of peak shape and full width by inserting an aperture at the DTIMS inlet that was used to control the neutral molecules' penetration into the separation region, thus preventing neutral-ion reactions inside. The FAPA and repeller's experimental operating conditions including drift and plasma gas flow rates, pulse injection times, repeller positioning and voltage, FAPA current, and effluent angle were optimized. Ion mobility spectra of selected compounds were captured, and the corresponding reduced mobility values were calculated and compared with the literature. The 6-fold improvements in limit of detection (LOD) compared with previous work were obtained for 2,6-DTBP and acetaminophen. The enhanced performance of the FS-FAPA-DTIMS was also investigated as a function of the GDE when compared with FAPA-DTIMS containing BNG.

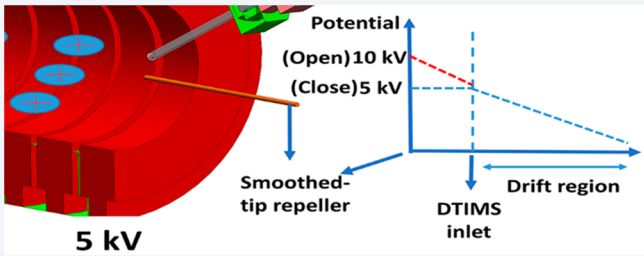


**KEYWORDS:** *drift tube ion mobility spectrometry, field-switching technique, flowing atmospheric-pressure afterglow, gate depletion effect, ambient desorption/ionization, Bradbury−Nielsen*

## 1. INTRODUCTION

Drift tube ion mobility spectrometry (DTIMS) is an analytical separation technique based on the ions' individual terminal velocity as they pass through a region with uniform electric field and drift gas performed mainly at atmospheric or subatmospheric pressure.[1] DTIMS has been widely used for detection of chemical warfare agents,[2,3] environmental contaminants,[4] narcotics,[5,6] aerosols,[7,8] proteomics investigations,[9−11] and gas-phase structural elucidations.[12,13]

DTIMS instruments typically implement an electrical ion gate, generally a Bradbury−Nielsen gate (BNG) or a Tyndall−Powell gate (TPG), between the reaction and drift regions.[14] The TPG is formed of two meshes where the center mesh is momentarily pulsed to allow ions into the drift region. The BNG is made up of a series of parallel wires connected to opposite potentials that create a perpendicular electric field relative to ion path and block the ions' entrance into the drift region for separation.[14] However, as the BNG wires' potential become identical, the blocking field is removed; hence, ions are allowed to enter into the drift region. In comparison with mechanical ion gates, like choppers, for generation of ion packets, BNG or TPG has a much faster speed in terms of opening and closing the gate.[14] Moreover, since the choppers should be conductive, isolation of the gate from the adjacent conductive rings that are connected to high voltage, as well as controlling the mechanical vibrations formed in the gate, is difficult.[15] Therefore, electrical ion gates are commonly deployed in IMS to generate discrete ions packet for separation. However, BNGs (and TPG to a higher degree in some cases) in DTIMS suffer several disadvantages, including intrinsic low duty cycle (1%),[1,16,17] physical ions loss on BNG surface wires,[1] gate depletion effect (GDE),[18,19] and difficulties pertinent to construction, such as the small inner distance among wires (<1 mm), especially if a high working temperature across the IMS cell is desired.[20,21]

One of the main issues associated with the BNG is the gate depletion effect (GDE) during injection into the drift region. When the closing potential is applied to the BNG wires at the end of the gating pulse, the electric field induced will "pull back" the ions that have not traveled a sufficient distance from the BNG plane.[18] In fact, electric field contour lines are extended on both sides of the BNG plane, and a larger number of ions with smaller mobility values will be pulled back and

Received: October 7, 2021
Revised: January 2, 2022
Accepted: February 22, 2022

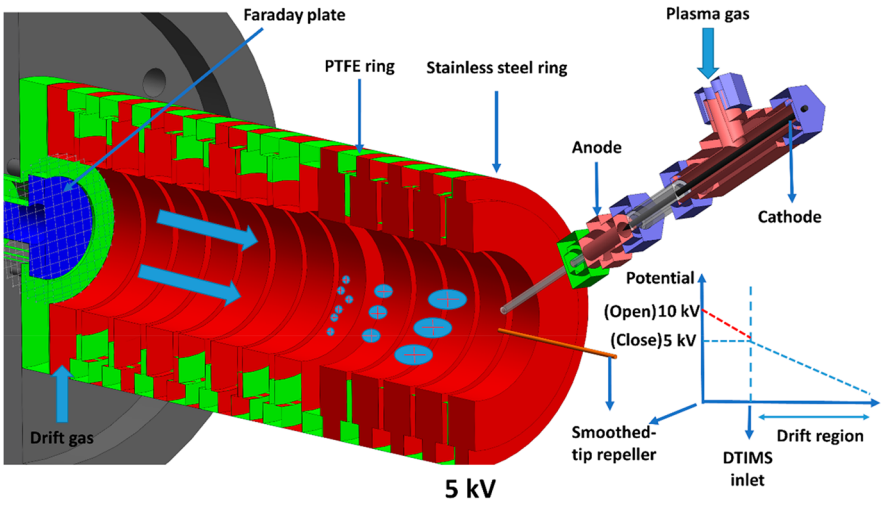


**Figure 1.** Field-switching FAPA-DTIMS experimental setup. The DTIMS inlet is biased to 5 kV while rounded-tip repeller is pulsed between 5 and 10 kV in order to accelerate ions formed in the FAPA source into the DTIMS cell for separation.

neutralized by the BNG. Overall, lower mobility ions will be lost due to this mobility-based discrimination effect affecting the quantitative aspect of the analysis. The GDE also depends on the closing voltage gradient between wires so that increasing the closing voltage results in further expanding the electric field and enlarging the GDE region of the BNG, decreasing the signal-to-noise ratio.[18] Moreover, in order to block the ions' entrance into the drift region during BNG closing time, the electric field between the BNG wires should be usually around 2−3-fold higher than the IMS cell electric field.[1] The applied electric field could be intensified either through applying higher voltage gradient between wires or decreasing inter wire distances. The former results in a considerable decrease in the peak intensity due to the GDE,[18,22] while the latter faces challenges related to the BNG design and construction as well as decreasing the signal intensity due to the lower gate transparency. It should also be noted that the GDE is more significant as the gate opening time becomes shorter, which is desirable for achieving higher resolution.[18] Also, in the portable and compact DTIMS, very short pulse injection times at the BNG are required.[23]

In addition, one of the main roles of the IMS drift gas is removing the memory effect from the analyte molecules that could be deposited on the IMS surfaces, including BNG wires. Thus, another issue with BNGs is that while volatile compounds are swept out of the IMS cell by the drift gas, lower volatility compounds could be deposited on the BNG wires. The deposition buildup over time will lead to the deterioration of the electric field in the BNG area and will adversely affect the ion transmission efficiency.[24]

The field-switching (FS) technique was first employed in DTIMS by Jenkins and Leonhardt et al. where the electric field in the ionization region was switched on and off, allowing the transportation of discrete measurable packets of ions into the separation region.[25,26] This method was further utilized by Kirk et al. where a metallic grid, called an "injection grid", was inserted between the ionization and drift region in order to send the discrete packet of ions into the drift region. Different ionization sources including radioactive sources,[25] ultraviolet (UV),[27] and X-ray[28,29] have also been coupled with the FS technique in DTIMS. However, since the FS requires a field-free region inside the ionization region, ionization sources like corona discharge (CD) and electrospray (ESI), which require the electric field for guidance, have not yet been coupled with the FS method in DTIMS, although they can be field switched in other cases such as electrical propulsion.[30,31] The tristate ion shutter was also proposed as an alternative method for the FSG technique to lower the GDE.[32] However, there is still a cutting width between two adjacent grids that acts against lower mobility ions. In addition, the nonlinear electric field that forms in the vicinity of the gate deviates the ion from its actual path and, hence, influences the ion's intensity and resolving power. In addition, in most studies, a mesh or grid was employed as the injection grid for ions transferring into the separation region, which lowers the ions' total current reaching the drift region and detector due to the optical transparency issue. In addition, Tabrizchi et al. combined the FS and BNG in order to improve the electric field strengths in the region behind the BNG, which enhances the signal-to-noise ratio obtained at the detector but suffers from the BNG issues.[33]

Therefore, here we propose a gridless field-switching gate (FSG) approach for coupling DTIMS with the ambient desorption/ionization sources that require a grounded electrode (electric field for ionization) in order to overcome the shortfalls related to the BNG. We previously demonstrated the coupling of one such source, a flowing atmospheric pressure afterglow (FAPA), with DTIMS via a tip-repeller electrode.[34] A similar approach was also utilized for coupling direct analysis in real time (DART) with DTIMS;[35] however, the tip-repeller electrode shape was modified in the more recent FAPA DTIMS[34] embodiment to enable application of significantly higher potentials before the onset of a secondary discharge, thus significantly improving ion transfer into the DTIMS. The FAPA source improves the portability potential of DTIMS due to the minimal sample preparation required, inherently higher plasma-gas temperature that facilitates desorption, and higher abundance, and a wider range of generated reagent ions compared to other ambient desorption ionization (ADI) techniques like low temperature plasma (LTP) and direct analysis in real time (DART).[34] The tip-repeller continuously deflected the desorbed/ionized analytes into the DTIMS reaction region featuring a BNG. The FSG proposed here, however, implements a high voltage pulse applied to the tip-repeller electrode to produce the discrete


https://doi.org/10.1021/jasms.1c00309
J. Am. Soc. Mass Spectrom. XXXX, XXX, XXX−XXX

ions packet accelerated into the DTIMS. The tip-repeller FSG is coupled to a FAPA source. An aperture was placed at the DTIMS inlet to minimize the penetration of neutral molecules into the drift region from the FAPA sampling region, thus removing significant background noise observed in the IMS spectra. In addition, the effect of DTIMS and FAPA source operating conditions on the signal intensity and resolution are presented. The optimum conditions are used to determine the quantitative figures of merit of selected analytes, including limits of detection (LOD). Finally, the improved performance of the tip-repeller FSG vs BNG, with respect to gate depletion effects, is characterized.

## 2. MATERIALS AND METHODS

**2.1. Chemicals.** 4-Acetamidophenol (98%), acetophenone (99%), heptanone (99%), butanone (99%), pentanone (99+ %), and dimethyl methylphosphonate (97%) were purchased from Alfa Aesar Co. (Ward Hill, MA). Methanol (LC/MS grade), 2,6-di-*tert*-butylpyridine (97%), and tetrabutylammonium iodide (98%) were purchased from Sigma-Aldrich Co. (St. Louis, MO). Water (ACS ChromAR grade) and glycerol (99.5+ %) were purchased from Macron Co. (Pittsburgh, PA). Methanol (LC/MS grade) was purchased from EMD Millipore Co. (Billerica, MA).

**2.2. Sample Preparation.** Regarding quantitative analysis, for 2,6-DTBP, 20 $\mu$L samples of standard solution with concentrations of 0.5−50 and 0.25−100 ppm were prepared by dilution of stock solutions in DI water for electric fields of 316 and 476 V/cm, respectively. The final concentrations of headspace samples were calculated based on the Raoult's law and directly injected in the desorption/ionization region (between repeller and DTIMS inlet). For acetaminophen, standard solutions with concentrations of 1−250 and 1−500 ppm were prepared with dilution of stock sample in methanol, and 6 $\mu$L of the sample was placed on the glass microfiber filter paper where it was subjected to the plasma plume for desorption/ionization.

**2.3. Flowing Atmospheric Pressure Afterglow Field-Switching Gate Drift Tube Ion Mobility Spectrometer.** The instrument previously described was modified to perform the studies here (Figure 1).[34] First, the original DTIMS BNG and reaction region were removed, which resulted in a modified drift region of 10.5 cm that starts at the DTIMS inlet. A smooth tip-repeller positioned coaxially at the DTIMS inlet facilitates the transmission of the ions produced by the FAPA source into the DTIMS by compensating for the opposite electric field formed between the FAPA-grounded anode and DTIMS inlet, which is biased to 5 kV (BERTAN, 205B-05R). In this configuration, the tip-repeller voltage is also biased to 5 kV (pulse offset), but it is pulsed to a higher potential (8.2−10.2 kV) in order to create a strong electric field to inject the packet of ions into the DTIMS. It was determined that 7 kV pulse voltage was the threshold to obtain ion current signal at the detector; thus, the repeller injection time is defined as the time when the pulse voltage was above 7 kV. This is achieved with a high voltage pulse switch (BEHLKE, HTS300), high voltage power supply (SPELLMAN, RHR10PN100), and a home-built pulse generator. The pulse frequency is set to 33 Hz, and the pulse duration studied ranged from 100 to 850 $\mu$s. The output of the HV pulser was monitored with a HV probe (Tektronix P6015A) in order to set the zero time for all DTIMS peak measurements and ensure that all gate pulses align exactly and set an identical zero time for all measurements. Table 1 summarizes the experimental operating conditions of field-switching FAPA-DTIMS. A glow discharge (GD) is achieved between a pin cathode and a Swagelok tube as the anode in a concentric geometry. The inner-electrode distance is 2.5 mm, and a glass capillary ($L$ = 4 cm, 1.56 mm i.d., 1.96 mm o.d.) extends from the anode in order to direct the generated ions from source into the sample for the desorption/ionization process. The capillary employed must be composed of an insulator in order to prevent any secondary discharge between source and DTIMS inlet biased to a high potential. The FAPA plasma operating gas was nitrogen, instead of the commonly deployed helium gas, in order to prevent a secondary discharge between the source and DTIMS inlet. The drift gas was passed through molecular sieves (13×) and entered into the drift region in the opposite direction of the ion path. A Faraday plate (25 mm diameter, brass) was chosen as the detector. As the ions reached the Faraday plate and collided with the surface, they lost their charge and the ion current was amplified by a home-built electrometer with a gain of $10^8$ connected to a digital oscilloscope (DSO-X 3034A, Agilent Technologies) for data collection.

**Table 1. Optimized Operating Conditions of Field-Switching FAPA-DTIMS**

| operating parameter | setting |
|---|---|
| drift electric field | 476 V cm$^{-1}$ |
| drift gas flow rate | 1640 mL min$^{-1}$ |
| repeller pulse width | 300 $\mu$s |
| repeller pulse frequency | 33 Hz |
| repeller opening voltage | 10 kV |
| repeller closing voltage | 5 kV |
| repeller distance from DTIMS inlet | 8 mm |
| DTIMS inlet aperture size | 2.5 × 5 mm |
| FAPA plasma current | 12 mA |
| FAPA plasma voltage | −695 V |
| FAPA plasma gas flow rate | 550 mL min$^{-1}$ |
| FAPA glass capillary/repeller angle | 80 deg |
| FAPA capillary tip distance to DTIMS inlet | 0 mm |

**2.4. Sample Introduction.** The liquid and solid samples were injected into the glass microfiber filter papers (3 mm diameter, 934-AH, Whatman) which were sandwiched between two glass pieces (3.5 mm × 75 mm × 2 mm). The loaded filter papers were placed at the IMS entrance, around 4 mm below the glass capillary and then were exposed to the plasma effluent gas for the desorption/ionization process.

## 3. RESULTS AND DISCUSSION

**3.1. Effect of DTIMS Inlet Aperture.** As Figure 1 shows, reagent ions generated by the FAPA source are accelerated into the drift region through a very high electric field of 6250 V/cm that exist in the 8 mm distance between repeller and aperture. Figure S.1 shows the FAPA DTIMS spectrum obtained for reagent ions or reactant ion peaks (RIP) in two different drift gases: nitrogen and helium. As Figure S.1 shows, changing the drift gas to helium reduces both full width (FW) and full width at half-maximum (fwhm) from 15 to 8.62 ms and 3.68 to 2.28 ms, respectively. When helium is employed as the drift gas, the degree of protonated water clusters (hydronium ions) formed in the drift region is reduced, which leads to a smaller FW observed as the tail in the DTIMS


https://doi.org/10.1021/jasms.1c00309
J. Am. Soc. Mass Spectrom. XXXX, XXX, XXX−XXX

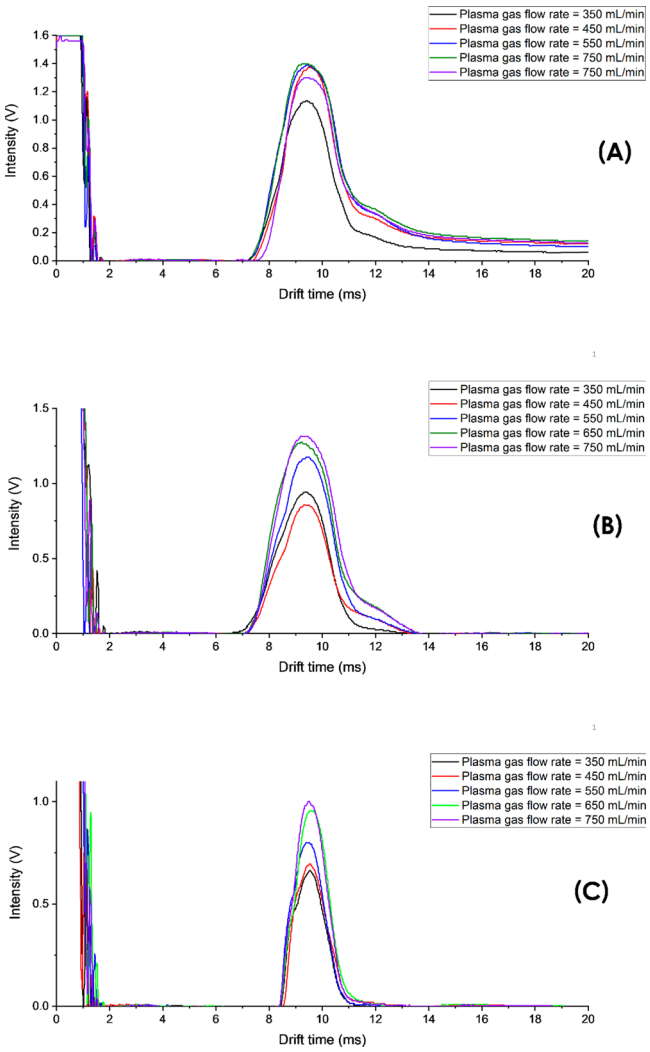


**Figure 2.** Ion mobility spectrometry of reagent ions obtained with a 7 × 7 mm aperture (A), a 5 × 5 mm aperture (B), and a 2.5 × 5 mm aperture (C).

peak. In fact, interconversion of high and low levels of hydronium ions are lowered in the entirety of drift region with utilization of helium as the drift gas, which is similar to a common phenomenon known as "ion stripping" between analyte and reactant ions, in the DTIMS.[1,36] Moreover, in comparison with nitrogen, helium has a much lower polarizability and collision cross section;[37] hence, according to Figure S.5.B, ions in the center are much less influenced by the drift gas and peak broadening becomes less noticeable. The peak intensities are around 1.24 and 2.92 V for nitrogen and helium, respectively; however, the observed long tail in the peaks leads to poor resolving power and prevents the separation of ions with similar mobilities. The long tail in the spectra is indicative of ions being generated inside the drift region. The FAPA glass capillary and DTIMS inlet have inner diameters of 2 and 30 mm, respectively; therefore the linear velocity of the FAPA effluent gas (2.91 m/s) is ∼100× higher than the drift gas (0.038 m/s). On one hand, the high linear velocity of the FAPA effluent gas results in better desorption efficiency as well as enhanced aerodynamic transport of analyte ions.[38] On the other hand, this also leads to the possible incursion of undesired neutrals (molecules desorbed, high energy reagents, etc.) from the FAPA plasma plume into the drift region. As a result, neutral molecules are ionized in the drift region through ionization mechanisms such as protonation, and the generated ions result in the long tail of the spectrum (Figure S.1). This effect is corroborated by a simulation of plasma gas flow implemented in the SolidWorks software, which is shown in Figure S.2. As Figure S.2 demonstrates, there is around a 2 cm penetration into the separation region of plasma gas effluent containing desorbed analyte neutral molecules as well as metastable species available in the plasma. According to Figure S.2, the plasma gas (simulated to be high-temperature nitrogen) is passed through a glass capillary with 2 mm diameter, hits the microfiber filter paper, and then enters the drift region. Regarding plasma gas flow simulation, the drift region length, plasma gas flow rate, and drift gas flow rate were 10 cm, 500 mL/min, and 1.64 L/min, respectively.

Apertures have been previously implemented in IMS to prevent diffusion of neutrals between different regions. For

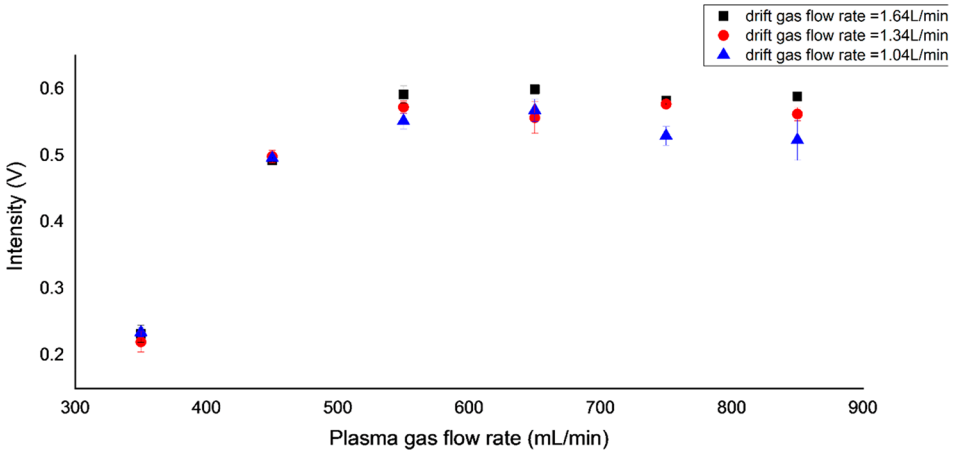


**Figure 3.** Effect of plasma gas flow rate on the obtained peak intensity of 2,6-DTBP at three different drift gas flow rates, including 1.64, 1.34, and 1.04 L/min. The drift electric field and repller voltage were set on 476 V/cm and 10 kV, respectively. The 3 $\mu$L of 2,6-DTBP and glycerol injected on a glass microfiber filter paper flushed with DTIMS inlet and oriented 50° relative to IMS axis (or repeller axis). There has been repeated samples for each data point.


https://doi.org/10.1021/jasms.1c00309
J. Am. Soc. Mass Spectrom. XXXX, XXX, XXX−XXX

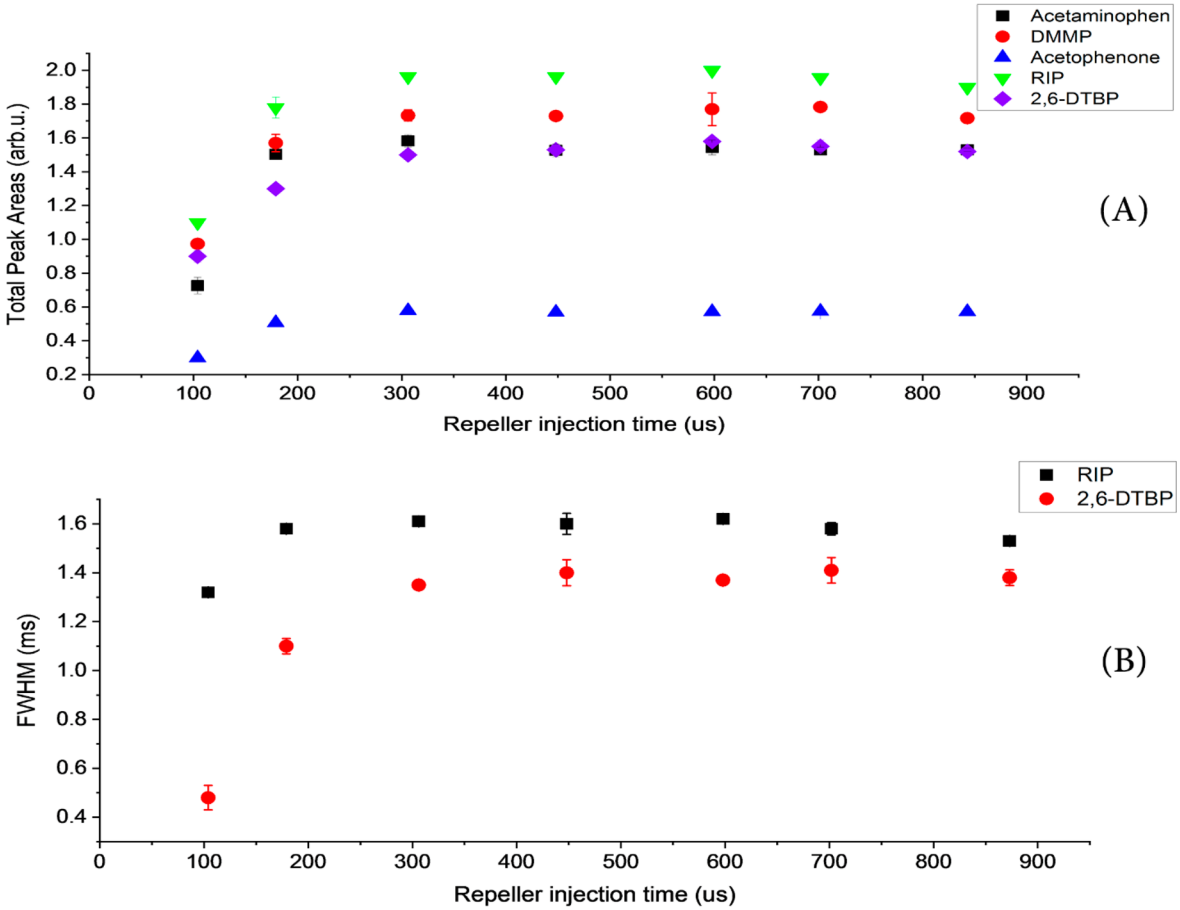


**Figure 4.** (A) Effect of repeller's pulse injection times on the total peak areas obtained for acetophenone, DMMP, 2,-DTBP, acetaminophen, and reagent ions. (B) Effect of repeller injection time on the fwhm of RIP and 2,6-DTBP. There have been repeated samples for each data point.

example, Tabrizchi et al. used two curtain electrodes with small diameters (around 2 mm i.d.) between the corona discharge electron source and the analyte ionization region, as well as a curtain gas flow, in order to prevent the penetration of neutrals from one region to the other.[39] Thus, better S/N was achieved because analyte molecules could not quench the corona discharge and neutral corona products could not suppress the ionization of analytes.[39] To mimic this effect in our FAPA DTIMS, an aperture was placed between the FAPA desorption/ionization region and the drift region. Figure S.3 shows a schematic of FAPA DTIMS which includes an aperture with dimensions of 2.5 × 5 mm. In this embodiment, no extra curtain gas is necessary because the significantly increased linear velocity of the drift gas at the aperture is used to keep the neutrals outside. The aperture is built into a glass microfiber filter paper (3 mm diameter, 934-AH, Whatman) attached to the DTIMS inlet, and three different dimensions (2.5 × 5 mm, 5 × 5 mm, and 7 × 7 mm) were used to study its effect on the resulting ion mobility spectra of reagent ions. A square/rectangular aperture allows changing the height independently of the width in a very simple and reproducible manner. The FAPA plasma gas flow rate was also varied between 350 and 750 mL/min.

Figure 2 plots the ion mobility spectrum of reagent ions obtained in different plasma gas flow rates ranging from 350 to 750 mL/min and three different apertures. The drift region electric field and drift gas flow rates were 476 V/cm and 1.64 L/min. In the case of a 7 × 7 mm aperture (Figure 2A), it is already clear that the fwhm of the reactant ion peak is improved compared to the case where no aperture is used (Figure S.1), even taking the drift tube field differences into account. Nevertheless, the RIP still shows a long tail that extends beyond 20 ms of drift time, which is indicative of ions forming in the drift region as a result of ion neutral molecule reactions. Reactant ions from the FAPA source are formed on the basis of the reactions described below:[40]

$$N_2 + e^- \rightarrow N_2^+ + 2e^- \quad (1)$$

$$N_2 + 2N_2 \rightarrow N_4^+ + N_2 \quad (2)$$

$$N_4^+ + H_2O \rightarrow H_2O^+ + N_4 \quad (3)$$

$$H_2O^+ + H_2O \rightarrow (H_2O)H^+ + OH^- \quad (4)$$

$$(H_2O)H^+ + M \rightarrow MH^+ + (H_2O) \quad (5)$$

Once nitrogen molecules are ionized through electron impact ionization (1), water molecules are ionized through charge exchange processes (2) and (3). Then hydronium ions are formed by protonation (4). As eq 5 shows, hydronium ions can react with neutral molecules M to yield protonated ions.

The linear velocity of plasma gas coming from FAPA glass capillary ranged from 1.85 to 3.97 m/s at the 350−750 mL/min flow rates. While the drift gas linear velocity at the 7 × 7 mm aperture (0.56 m/s at 1.64 L/min) is more than an order of magnitude higher compared to the fully open DTIMS inlet (0.038 m/s), it is still significantly lower than the linear


https://doi.org/10.1021/jasms.1c00309
J. Am. Soc. Mass Spectrom. XXXX, XXX, XXX−XXX

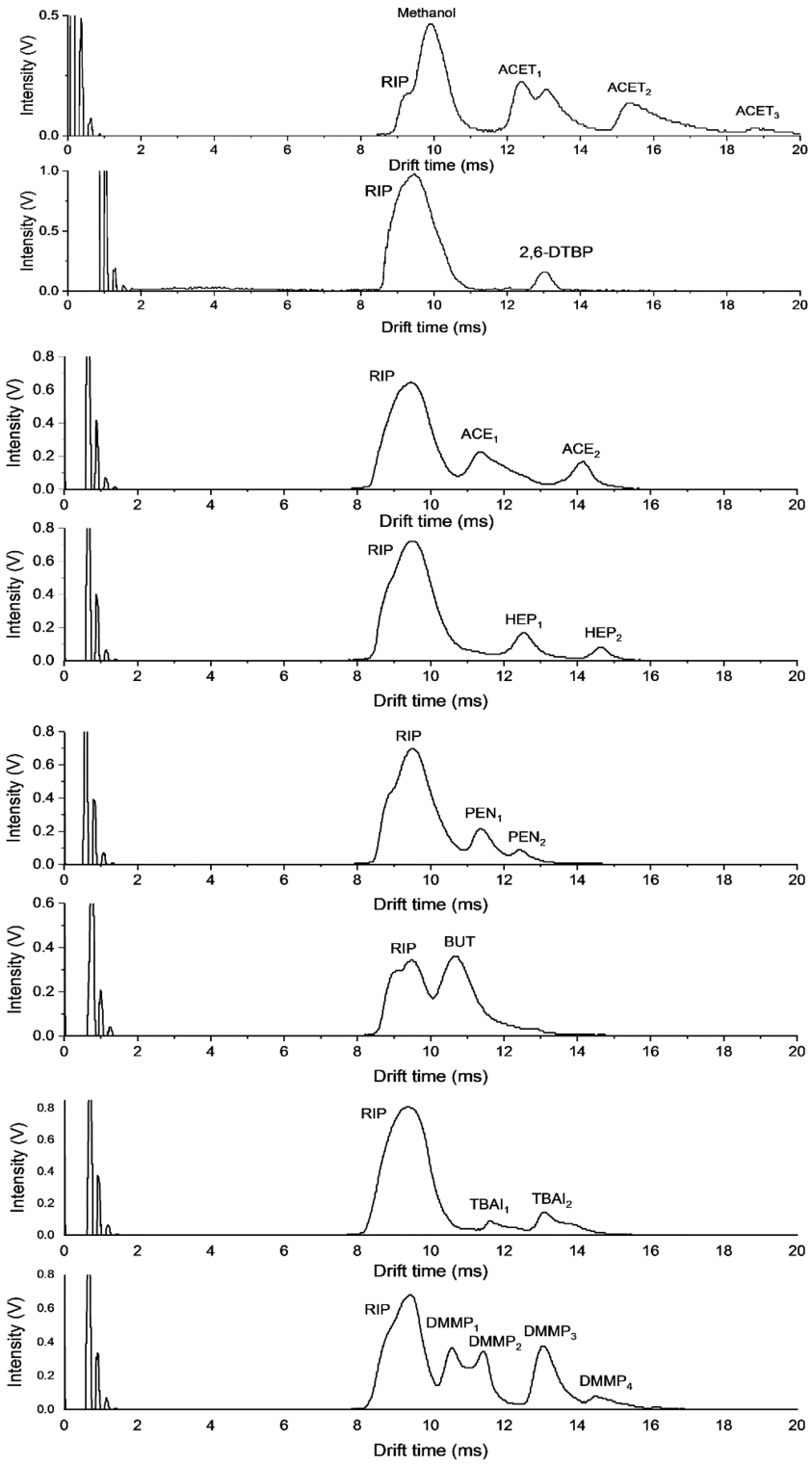


**Figure 5.** Ion mobility spectra of selected compounds including 2,6-DTBP, acetaminophen, acetophenone, heptanone, pentanone, butanone, TBAI, and DMMP.

velocity of the FAPA effluent (1.85−3.97 m/s). Thus, it is reasonable to expect that neutral and metastable species available in the desorption/ionization region, such as the $H_2O$, $N_2$, and $N_2$*, will still be able to penetrate into the drift region, creating the protonation reactions (eq 5).

Further decreasing the aperture size to 5 × 5 mm increases the obtained drift gas linear velocity to 1.09 m/s, which results in a further decrease of neutral molecules penetrating into the drift region, significantly narrowing the peak tail (Figure 2B). Also, it is evident that increasing the FAPA plasma gas flow rates results in greater signal peak intensities, which may be due to improved aerodynamic transport of ions into the IMS cell.[41] For instance, the RIP peak intensity is increased from 0.85 to 1.3 V as plasma flow rates are raised from 350 mL/min (1.85 m/s) to 750 mL/min (3.97 m/s), while the peak full width increases from 6 to 6.4 ms. The smallest aperture tested


https://doi.org/10.1021/jasms.1c00309
J. Am. Soc. Mass Spectrom. XXXX, XXX, XXX−XXX

**Table 2. Reported Reduced Mobility Values ($K_0$) Obtained with Field-Switching FAPA-DTIMS and Other Ionization Sources**

| compd | product ion peak | $K_0$ ($cm^2$ $V^{-1}$ $s^{-1}$) this work | $K_0$ ($cm^2$ $V^{-1}$ $s^{-1}$) ref value |
|---|---|---|---|
| 2,6-di-*tert*-butylpyridine (2,6-DTBP) | 2,6-DTBP | 1.40 | 1.41 (FAPA),[34] 1.42 (ESI),[44] 1.42 (CD)[43] |
| acetaminophen | ACET1 | 1.47 | 1.37 (FAPA)[34] |
| | ACET2 | 1.19 | 1.10 (FAPA)[34] |
| | ACET3 | 0.97 | |
| acetophenone | ACE1 | 1.59 | 1.82 (UV)[39] |
| | ACE2 | 1.28 | |
| heptanone | HEP1 | 1.45 | 1.62 ($^{63}$Ni)[46] |
| | HEP2 | 1.24 | 1.48 ($^{63}$Ni)[46] |
| butanone | BUT | 1.70 | 1.86 [UV],[39] 2.05 (50 MBq)[47] |
| pentanone | PEN1 | 1.60 | 1.58 ($^{63}$Ni)[46] |
| | PEN2 | 1.46 | 1.46 ($^{63}$Ni)[46] |
| dimethyl methylphosphonate (DMMP) | DMMP1 | 1.72 | 1.81 (LTP)[41] |
| | DMMP2 | 1.58 | 1.44 (LTP)[41] |
| | DMMP3 | 1.39 | |
| | DMMP4 | 1.25 | |
| tetrabutylammonium ioide (TBAI) | TBAI1 | 1.56 | |
| | TBAI2 | 1.36 | |

was 2.5 mm × 5 mm, which completely accommodates the cylindrical repeller (2.5 mm diameter), sample desorption substrate (filter paper), and FAPA capillary (~2 mm o.d.). This aperture provides the highest linear velocity (2.18 m/s) for the drift gas, which is within the range of working plasma gas linear velocities (1.85−3.97 m/s). As Figure 2c shows, this smallest aperture improved the obtained fwhm (1.52 to 1.40 ms, for 350 to 750 mL/min plasma gas) compared to the larger apertures. The overall peak intensities are lowered compared to the larger apertures, but they are seen to improve from 0.66 to 1.00 V as the plasma gas flow rate is increased. Moreover, a simulation of plasma gas flow trajectories was implemented in order to investigate the penetration of plasma gas effluent containing the metastable species and neutral molecules into the drift region as shown in Figure S.4. Inserting an aperture at the DTIMS inlet prevents diffusion of plasma gas effluent into the separation region due to the higher drift gas linear velocity when compared with a DTIMS inlet without aperture and large diameter (30 mm) (Figure S.4).

In addition, ion velocity in IMS is influenced by the electric field inside the IMS cell as well as drift gas velocity.[40] Thus, the simulation of drift gas flow inside the IMS cell (with 30 mm diameter) was completed, and a random plane (located at 48.5 mm from DTIMS inlet) was selected in order to investigate the radial distribution of drift gas velocity within the selected plane

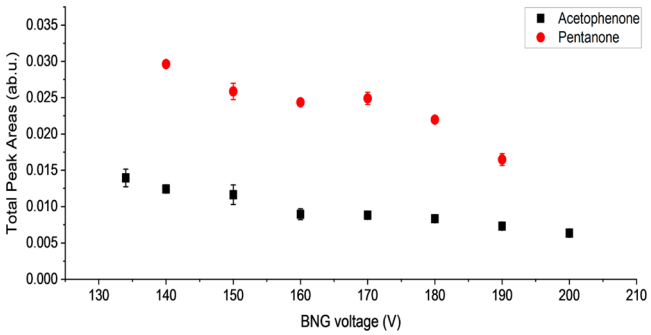


**Figure 6.** Total peak areas obtained for acetophenone and pentanone as a function of BNG voltage.

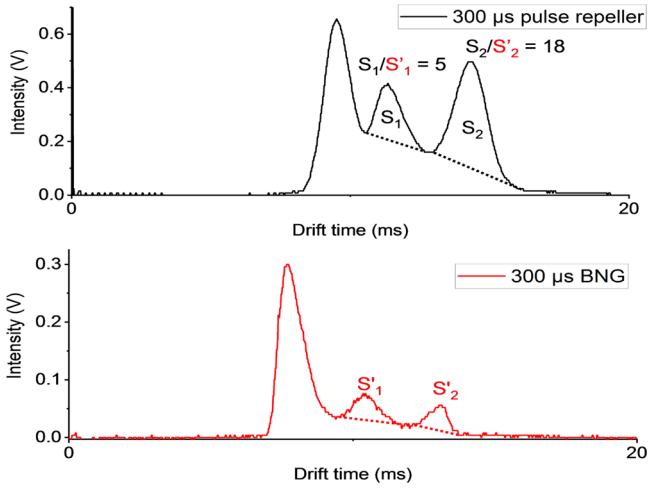


**Figure 7.** Ion mobility spectra of acetophenone under two different pulsing methods including BNG and pulsing the repeller (300 $\mu$s). The $S_1$ and $S_2$ are the peak areas above the dashed lines for the first and second peak, where packet of ions are formed by pulsing the repeller. The $S'_1$ and $S'_2$ are the peak areas above the dashed lines for the first and second peak, where packet of ions are formed by pulsing the BNG.

for two cases, an aperture with a 2.5 × 5 mm dimension and no aperture (Figure S.5). As Figure S5.B shows, when there is no aperture at the DTIMS inlet, the drift gas linear velocity, in the center of IMS cell, is around 1 order of magnitude higher (0.2 m/s), compared with the one with an aperture (0.02 m/s, Figure S5.A). In addition, considering the drift region length (10.5 cm) and ion drift time (~10 ms), ions have a velocity of ~1 m/s. Thus, by inserting an aperture, the IMS peak broadening becomes less problematic. From the SIMION simulation described in Figure S.6, ions moving in the center of IMS axis experience a more uniform electric field than the ions near the IMS walls. Inserting an aperture, therefore, allows a

**Table 3. Comparison of Analytical Figure of Merits between FAPA-Shutterless DTIMS and Our Previous Work (Containing BNG)**

| compd | linear dynamic range: this work | linear dynamic range: previous work | limit of detection: this work | limit of detection: previous work | correlation of coefficient ($R^2$): this work | correlation of coefficient ($R^2$): previous work |
|---|---|---|---|---|---|---|
| 2,6-DTBP | 8.7−870 ppb | 21−1050 ppb | 3.78 ppb[a] | 18 ppb | 0.99 | 0.97 |
| | 4.3−1740 ppb | | 3.02 ppb[b] | | 0.99 | |
| acetaminophen | 0.006−1.5 $\mu$g[a] | 0.06−1.5 $\mu$g | 5 ng[a] | 30 ng | 0.99 | 0.99 |
| | 0.006−3 $\mu$g | | 4 ng | | 0.99 | |

[a]Electric field = 316 V/cm. [b]Electric field = 476 V/cm.


https://doi.org/10.1021/jasms.1c00309
J. Am. Soc. Mass Spectrom. XXXX, XXX, XXX−XXX

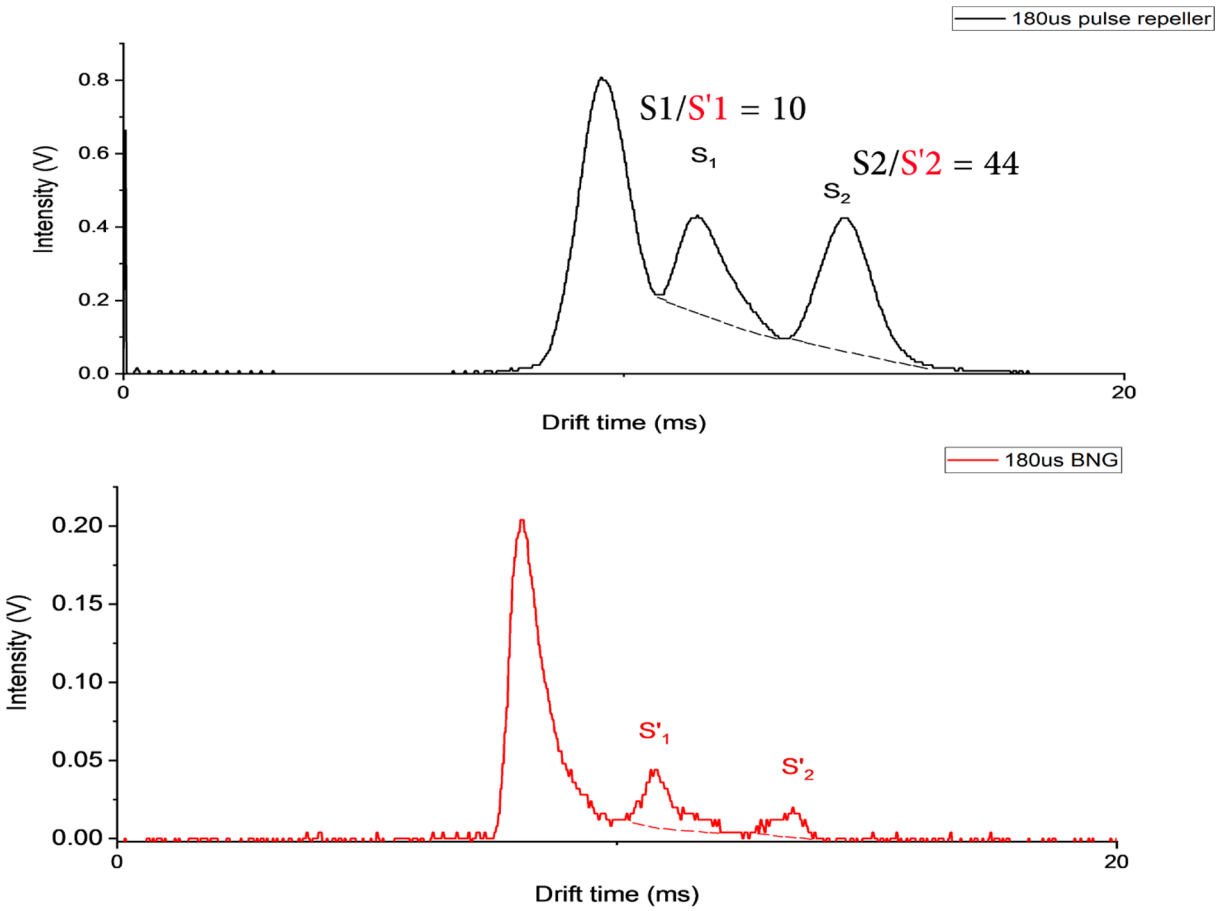


**Figure 8.** Ion mobility spectra of acetophenone under two different pulsing methods including BNG and pulsing the repeller (180 $\mu$s). The $S_1$ and $S_2$ are the peak areas above the dashed lines for the first and second peak, where packets of ions are formed by pulsing the repeller. The $S'_1$ and $S'_2$ are the peak areas above the dashed lines for the first and second peak, where packets of ions are formed by pulsing the BNG. Table 2 reports all obtained peak area for acetaminophen peaks for two different pulse injections of 180 and 300 $\mu$s applied by BNG and pulse repeller.

**Table 4. Peak Areas Obtained for Acetophenone under Two Different Pulse Injections Methods including BNG and Pulse Repeller (180 and 300 $\mu$s)**

| | peak area | | | |
|---|---|---|---|---|
| | pulse repeller | | pulse BNG | |
| pulse injection time ($\mu$s) | first peak ($S_1$) | second peak ($S_2$) | first peak ($S'_1$) | second peak ($S'_2$) |
| 180 | 0.27 | 0.42 | 0.02 | 0.01 |
| 300 | 0.21 | 0.52 | 0.04 | 0.03 |

centered and denser packet of ions to be injected into the drift region leading to the peak broadening becoming less noticeable.

Regarding the effect of the electric field on the ion neutral reactions, a DTIMS spectrum was obtained for RIP in an electric field of $E$ = 620 V/cm. As Figure S.7 shows, increasing the electric field lowers the full width from 15 to 10.36 ms. Although the reduction in full width is considerable, the resulting full width is still too large and impedes a qualitative analysis, possibly due to the large area (around 2 cm of the drift region as Figure S.2 shows) of the drift region where plasma reagent species and desorbed neutral molecules diffuse, which still allows enough time for post ionization and reaction mechanisms. The reduction in full width is attributed to the lower reaction time provided for ion and neutral molecules in the drift region, as the electric field is increased.

**3.2. Effect of Drift Gas and Plasma Gas Flow Rates.** As discussed in the previous section, the linear velocity of the drift gas at the DTIMS inlet has a significant effect on the IMS spectra shape given that the FAPA plasma gas flows in the opposite direction. To study the effect of the velocity of the drift gas, its flow rate was varied from 1.64 L/min (2.18 m/s) to 1.34 L/min (1.78 m/s) and 1.04 L/min (1.38 m/s). In addition, the FAPA plasma gas flow rate influences the sample desorption and transport of ions into the DTIMS cell.[34] Thus, the FAPA plasma gas flow rate was changed between 350 mL/min (1.85 m/s) to 850 mL/min (4.50 m/s) to study its effect on the DTIMS spectra of 2,6-DTBP and glycerol.

Figure 3 shows the peak intensity of 2,6-DTBP as a function of plasma gas flow rate for the three drift velocity cases. In general, a considerable rise in the peak intensity is obtained as plasma gas flow rates are increased from 350 mL/min (0.234 V) to 550 mL/min (0.593 V), where it plateaus until 850 mL/min (0.590 V). This trend is very similar the one obtained for a FAPA coupled to a BNG DTIMS in to our previous work, but there is a significantly higher peak intensity (~×10) with the tip repeller FSG DTIMS here.[34] Increasing the plasma gas flow rate will enhance the density of the available reagent ions; hence, a larger number of analyte molecules can be ionized, which results in increased peak intensity. The plateau observed between 550 to 850 mL/min could be due to the reduction of the residence time of analytes and reagent ions in the reaction


https://doi.org/10.1021/jasms.1c00309
J. Am. Soc. Mass Spectrom. XXXX, XXX, XXX−XXX

volume, which would balance the effect of having a higher concentration of reagents at higher flow rates.

Moreover, the effect of plasma gas flow rate on the obtained fwhm for 2,6-DTBP in three different drift gas flow rates were investigated as shown in Figure S.8. It is evident that increasing the plasma gas flow rate results in a corresponding raise in the obtained fwhm for 2,6-DTBP in all three working drift gas flow rates and where the smallest drift gas velocity in general corresponds to the largest fwhm. Also in the inset of Figure S.8, the DTIMS spectra of 2,6-DTBP are shown in two different plasma gas flow rates of 350 and 850 mL/min, with a drift gas flow rate of 1.04 L/min. In fact, two separate peaks are observed for each case including RIP and 2,6-DTBP. For instance, when the plasma gas flow rate is 350 mL/min, both peaks are present in the spectra, since the concentration of 2,6-DTBP is not high enough to completely deplete the reactant ions. Increasing the plasma gas flow rate improves the desorption efficiency and transportation of ions into the drift region, so a larger amount of analyte ions could be formed through ionization mechanism like protonation; hence, a larger number of reactant ions are consumed by the analyte and a reduction in the corresponding RIP intensity is observed. Matching of the arrival times for both RIP and analyte, at different plasma gas flow rates, confirms the reproducibility of analyte ions in terms of reduced mobility (drift time).

In the case of glycerol, given in Figure S.9, a similar trend as that of 2,6-DTBP is observed in the peak intensity, where it increases with plasma gas flow rate to a plateau. For example, at a drift gas flow rate 1.64 L/min, the peak intensity is increased from 0.43 to 0.63 V when varying the plasma gas flow rate from 350 to 550 mL/min where it plateaus, which is the same inflection point as in the case of 2,6-DTPB. At a drift gas flow rate = 1.34 L/min, however, the peak intensity reaches a plateau at a higher plasma gas flow rate 650 mL/min and results in higher peak intensities (0.87 V). It should be noted that in the case of 2,6-DTBP there were no discernible differences in the peak intensities obtained at different drift gas flow rates (Figure 3). The 2,6-DTBP has a very high vapor pressure (39 Pa) such that it does not need an efficient desorption induced by the FAPA effluent for the analyte to be available for ionization. On the other hand, glycerol has a significantly lower vapor pressure (0.01 Pa), such that its sampling relies heavily on the effectiveness of the FAPA desorption process. Thus, it follows that most of the differences in peak intensity observed for glycerol at different drift gas/plasma gas flow rates are due to effects on the desorption processes. In turn, this indicates that the higher linear velocities of the drift gas at the DTIMS inlet affect the desorption process of the analytes from the adjacent sample substrate, all of which depend on the plasma gas flowing in the opposite direction. For example, the highest drift gas flow rate at 1.64 L/min would affect these processes the most and would not permit a higher peak intensity above the 550 L/min plasma−gas flow rate. Conversely, increasing the plasma gas flow rate to 650 L/min still affords an increase in peak intensity at a drift gas flow rate of 1.34 L/min. Unlike our previous work,[34] increasing the plasma gas flow rate improves the obtained signal intensities, which may be partially due to the higher concentration of glycerol used in this work (1050 ppm vs 800 ppm) and partially to a higher reaction time among analyte molecules and reactant ions obtained with a higher reaction volume available in the desorption/ionization region (around 8 mm vs 4 mm in the previous configuration). At the lowest drift gas flow rate, 1.04 L/min, the trend is completely different, which could be due to the increasingly dominant effect of unwanted neutrals penetrating into the drift region, supported by the change in the calculated reduced mobility value of glycerol which varied between 1.32 to 1.8 $cm^2\ V^{-1}\ s^{-1}$ once the plasma gas flow rate is changed between 350 to 850 mL/min, while the calculated reduced mobility value of glycerol was $cm^2\ V^{-1}\ s^{-1}$ during all working plasma gas flow rates once the drift gas flow rate is set on 1.64 L/min. (plasma gas flow rate = 350 − 850 mL/min).

**3.3. Effect of Pulse Injection Time.** The effect of repeller's pulse injection time on the obtained total peak areas were examined for four analytes including dimethyl methyl phosphonate (DMMP), 2,6-DTBP, acetophenone, acetaminophen, and reagent ions. For sample preparation, 2 μL of DMMP, 2,6-DTBP, and acetophenone, as well as 2.5 μL of acetaminophen, were injected on the glass microfiber filter paper. The operating electric field, repeller voltage, FAPA plasma current, capillary effluent angle, and the repeller distance from DTIMS inlet were set according to Table 1. For each analyte, the total area for all peaks in the spectra was calculated and plotted as a function of pulse injection times that varied between 104 and 843 μs as shown in Figure 4A. There is a considerable increase in the obtained total peak area for all analytes as the injection time is increased from 104 to 306 μs, and a plateau trend is observed following 306 μs and extended to 843 μs. For example, the 2,6-DTBP total peak area is increased by 1.6 times, while for reagent ions and DMMP, the total peak areas are increased 1.78 times between 104 and 306 μs. In addition, 2.19- and 1.96-fold increments are observed in the case of acetaminophen and acetophenone, respectively. For all three analytes, 306 μs was chosen as the optimum amount for the repeller's pulse injection time. In other words, using 306 μs as the injection time provides enough time for all of the ions formed in the ionization region to enter into the drift region with an operating electric field of 6250 V/cm between repeller and DTIMS inlet. The injection times lower than 306 μs lead a decrease in the total peak areas due to the electric field cessation.

Figure 4B demonstrates the effect of repeller injection time on the fwhm of RIP and 2,6-DTBP. As Figure 4B shows, as the pulse width is increased from 104 to 306 μs, there is a considerable increase in the fwhm from 1.32 to 1.61 ms for RIP. A similar trend is also observed for 2,6-DTBP with a corresponding increase in the fwhm from 0.48 to 1.35 ms. Increasing the opening time, in fact, accelerates larger amounts of ions into the separation region, increasing fwhm. However, from 306 μs up to 873 μs, there is a plateau trend and fwhm remains almost unchanged for RIP and 2,6-DTBP, respectively. The plateau of both peak intensity and fwhm as a function of increasing repeller injection time indicates that there is complete depletion of generated ions in the desorption/ionization region within pulse widths >306 μs; otherwise, the peak intensity and fwhm should have kept increasing.

**3.4. Repeller Positioning and Voltage Optimizations.** The signal dependence of 2,6-DTBP as a function of repeller distance and voltage was investigated (Figures S.10 and S.11). In this experiment, drift electric field, FAPA effluent angle, and FAPA plasma current were set to the amounts shown in Table 1. For sample preparation, 3 μL of 2,6-DTBP was injected on a glass microfiber filter paper. After each injection, the peak intensities of reagent ions declined, while the peak intensity of


https://doi.org/10.1021/jasms.1c00309
J. Am. Soc. Mass Spectrom. XXXX, XXX, XXX−XXX

analyte (2,6-DTBP) increased and reached a maximum amount at which the IMS spectra were captured.

Figure S.10.A shows the obtained peak intensity of 2,6-DTBP as a function of the distance between repeller and DTIMS inlet (FAPA capillary was fixed at 0 mm distance from DTIMS inlet). According to Figure S.10.A, as the repeller approaches the inlet varying from 12 to 8 mm, the obtained signal intensity was increased from 0.32 to 0.47 V. In fact, this results in an increase in the electric field in the desorption/ionization region which improves the ion-transport efficiency into the DTIMS and leads to a corresponding increase in the obtained signal intensity. However, a significant decline of 1.67-fold is monitored as the repeller distance changes from 8 to 6 mm. The downward trend continues to 2 mm, where the obtained peak intensity is 0.064 V. It is speculated that the much higher electric fields may eventually lead to a significant decrease in the reaction time between reagent ions and desorbed analyte molecules in the region, which would lead to poorer ionization resulting in decreasing the signal intensities for 2,6-DTBP. This is supported by the higher RIP peak intensity observed at shorter distances (see Figure S.10.B inset). In comparison with our previous work in which the peak intensity improved by approaching the repeller to the inlet, but suffered a decline after 4 mm,[34] the peak intensity declines in this case after 8 mm significantly since the aperture inserted at the inlet narrows the total amount of ions entering the separation region.

In addition, the effect of repeller distance on the fwhm for 2,6-DTBP was obtained and plotted in Figure S.10.B. According to Figure S.10.B, as the repeller approaches the DTIMS inlet, fwhm deteriorates. For example, reducing the distance from 12 to 2 mm, leads to a corresponding increase in fwhm from 1.1 to 1.92 ms. In fact, deterioration of fwhm is correlated to the ion stripping formed as a result of dissociation reactions of analyte ions with reactant ions in the drift region (Figure S.10.B inset).[1,36] Also, once the repeller distance is set to 2 mm away from the DTIMS inlet, two peaks in the RIP are observed, which could be related to different water-cluster size hydronium ions $(H_2O)_n H^+$ or other species like $(H_2O)_n NO^+$ and $(H_2O)_n NH_4^+$, which are common reactant ions that could be formed in the DTIMS.[40]

The repeller voltage determines the electric field in the ionization region and influences the obtained signal intensity. According to Figure S.11, there is almost a linear increase in the peak intensity as repeller voltages is increased from 8.2 to 9.6 kV, followed by a plateau trend past 10 kV (5 kV above the DTIMS inlet voltage), corroborating our previous studies.[34] Increasing the voltage from 8.2 to 9.6 kV leads to a corresponding increase in the peak intensity from 0.02 to 0.60 V. Increasing the repeller voltage enhances the existing electric field that accelerates ions into the drift region resulting in a rise in the obtained peak intensity. However, further increasing the voltage (up to 10 kV is shown) leaves the peak intensity unchanged due to the fact that all generated ions in the desorption/ionization region already would have entered the drift region using lower voltages.

**3.5. FAPA Effluent Capillary Angle Optimization.** The orientation of the FAPA capillary relative to the sample not only affects the sample desorption rate[38] but also determines the effective ion transportation into the drift region. According to Table 1, 2 $\mu$L of 2,6-DTBP was injected on the glass microfiber filter paper while the FAPA effluent angle was varied from 80° to 60° (Figure S.12). Decreasing the angle from 80° to 70° results in a mild decline in peak intensity, ~3.5% for 2,6-DTBP and ~25% for the RIP, following the same trend as was observed in the case of FAPA BNG DTIMS.[34] Further decreasing the angle to 60° increases the 2,6-DTBP peak intensity but also increases the fwhm and leads to a constant elevated background of ~0.16 V. The elevated background is probably due to the aerodynamic transport of ions into the DTIMS cell even in the absence of the tip-repeller electric field during FSG off time. In other words, although during the off time there is not an electric field in the desorption/ionization region, ions are still transported into the drift region due to the FAPA effluent gas flow rate. Therefore, 80° was chosen as the optimum amount for the FAPA effluent capillary angle. Although it is preferable to set the operating FAPA angle to 90°, given the experimental geometry restrictions, the maximum angle obtainable was 80° while keeping the FAPA capillary tip at the optimum of 0 mm from the DTIMS inlet.

**3.6. FAPA Plasma Current Optimization.** FAPA plasma current and temperature have an influence on the abundance and range of ions formed through different ionization mechanisms as well as on the plasma gas temperature for desorption.[42] Therefore, peak intensities of 2,6-DTBP as a function of plasma currents varying between 12 and 20 mA were examined, and operating conditions were adjusted as described in Table 1. Plasma currents below 12 mA make the plasma unstable. For sample preparation, 2 $\mu$L of 2,6-DTBP was placed on the filter paper. After each injection of the analyte, an increase in the peak intensity was observed until it reached a maximum amount where IMS peaks were captured, and peak intensities were calculated (Figure S.13). Following Figure S.13, there is almost a linear decline in the peak intensities as the plasma current increases from 12 to 20 mA, similar to what was observed previously.[34] For instance, the peak intensity declines from 0.58 to 0.11 V as the plasma current is raised from 12 to 20 mA. Although increasing the plasma current leads to higher plasma gas temperature, improving the desorption and forming a greater abundance of reagents ions at the source, it also leads to larger charge exchange and a lower number of protonated water clusters from the RIP that are generated, consequently leading to a lower number of analyte ions that are formed through the protonation ionization mechanism.[34,42]

**3.7. Ion Mobility Spectra.** In order to investigate the capability of the instrument for identification and determination, a wide range of compounds in terms of mobility values were selected and ion mobility spectra were calculated (Figure 5) and reported in Table 2. The main purpose is to provide a rough estimate of $K_0$ values obtained with the FAPA source and FSG repeller technique. In this experiment, 2,6-DTBP was chosen as the standard to calculate the reduced mobility values ($K_0$) of other analytes. The experimental operating conditions were adjusted according to Table 1. Regarding sample introduction, 2 $\mu$L of each analyte was injected on the glass microfiber filter paper and then subjected to FAPA plasma plume for desorption/ionization. Several pulses (rings) observed at the beginning of spectrum around the time of the high voltage pulse are due to parasitic currents originating from parasitic capacitance that exist among all connections (at different voltages).

For 2,6-DTBP, a single peak at 13.12 ms is observed with a corresponding $K_0$ value of 1.40 $cm^2\ V^{-1}\ s^{-1}$, which is assumed to correspond to the protonated monomer of 2,6-DTBP. The


https://doi.org/10.1021/jasms.1c00309
J. Am. Soc. Mass Spectrom. XXXX, XXX, XXX−XXX

calculated $K_0$ value is consistent with the ones obtained with the original FAPA-DTIMS configuration featuring a BNG ($K_0$ = 1.41),[34] CD-DTIMS ($K_0$ = 1.42),[43] and ESI-DTIMS ($K_0$ = 1.42).[44] In the case of acetaminophen, three peaks are obtained at 12.46, 15.41, and 18.87 ms, with corresponding $K_0$ values of 1.47, 1.19, and 0.97 $cm^2\ V^{-1}\ s^{-1}$, respectively (labeled $ACET_1$, $ACET_2$, and $ACET_3$). In our previous work (FAPA-DTIMS with BNG), two peaks for acetaminophen with $K_0$ values of 1.37 and 1.10 $V\ cm^{-1}\ s^{-1}$ were obtained.[34] The difference in the calculated reduced mobilities for acetaminophen between FAPA-DTIMS and field-switching FAPA-DTIMS could be correlated to the different reaction time among reagent ions and neutral molecules in two different geometries since the reaction volume is different. In addition, the generated RIP peak for acetaminophen is different from other selected compounds due to the different solvent used for acetaminophen (methanol).

Acetophenone displays distinct peaks (labeled with $ACE_1$ and $ACE_2$) with $K_0$ values of 1.59 and 1.28 $cm^2\ V^{-1}\ s^{-1}$. A $K_0$ value of 1.82 $cm^2\ V^{-1}\ s^{-1}$ was reported for acetophenone with a hydrogen discharge lamp as the ionization source.[45] For heptanone, two peaks ($HEP_1$ and $HEP_2$) were observed at 12.53 and 14.64 ms (with $K_0$ values of 1.45 and 1.24 $cm^2\ V^{-1}\ s^{-1}$, respectively). In the literature, two $K_0$ values of 1.62 and 1.48 $cm^2\ V^{-1}\ s^{-1}$ were reported for heptanone, where $^{63}Ni$ was utilized as the ionization source.[46] Butanone gives a single peak at 10.66 ms (labeled with BUT) with a corresponding $K_0$ value of 1.70 $cm^2\ V^{-1}\ s^{-1}$, compared with $K_0$ values of 2.05 and 1.86 $cm^2\ V^{-1}\ s^{-1}$ that were obtained for butanone with a hydrogen discharge lamp and tritium (50 MBq) as ionization sources, respectively.[39,47] Regarding pentanone, there are two distinct peaks (labeled with $PEN_1$ and $PEN_2$) with calculated $K_0$ values of 1.60 and 1.46 $cm^2\ V^{-1}\ s^{-1}$, respectively, which are in close agreement with reported $K_0$ values of 1.58 and 1.46 $cm^2\ V^{-1}\ s^{-1}$ obtained with $^{63}Ni$ as the ionization source.[46] The DMMP produces four separate peaks at 10.56, 11.46, 13.06, and 14.50 ms (labeled as $DMMP_1$, $DMMP_2$, $DMMP_3$, $DMMP_4$ in Figure 5) with $K_0$ values of 1.72, 1.58, 1.39, and 1.25 $cm^2\ V^{-1}\ s^{-1}$, respectively, compared with $K_0$ values of 1.81 and 1.44 $cm^2\ V^{-1}\ s^{-1}$ obtained with a low-temperature plasma as the ionization source.[41] Tetrabutylammonium iodide (TBAI) also gives two peaks with $K_0$ values of 1.56 and 1.36 $cm^2\ V^{-1}\ s^{-1}$ (labeled with $TABI_1$ and $TBAI_2$).

**3.8. Analytical Figure of Merits.** The analytical figures of merit (FOM) were obtained from calibration curves for 2,6-DTBP in the gas phase and acetaminophen in the solid phase under two different drift electric fields of 316 V/cm (Figures S.14 and S.16) and 476 V/cm (Figures S.15 and S.17). The FOMs in the electric field of 316 V/cm were obtained in order to provide a comparison with our previous work (FAPA-DTIMS containing BNG). The limit of detection (LOD = 3.3 × Sb/$m$, Table 3) was determined from the standard deviation of the background (Sb) and the slope of the calibration curves ($m$). For 2,6-DTBP (Figures S.14 and S.15), an LOD of 3.78 ppb was determined for an electric field of 316 V/cm, with a corresponding linear dynamic range of 8.7−870 ppb, compared with the LOD = 18 and 21−1050 ppb that were previously reported for FAPA DTIMS with BNG.[34] Increasing the electric field to 476 V/cm yields some improvement in LOD (3.02 ppb) and a significantly improved linear dynamic range (4.35−1740 ppb). In fact, increasing the electric field provides a higher amount of reagent ions (primary ions) for analyte molecules to be ionized and fully deplete the reagent ions (through protonation); hence, the upper boundary of the linear dynamic range is improved.

Regarding acetaminophen, the total peak areas were calculated and used to plot the calibration curves (Figures S.16 and S.17). For high concentrations of acetaminophen, three distinct peaks are obtained, so after the injection and the wait for the maximum peak intensities, peak areas under each peak were calculated and the sum of the peak areas were considered as the response and plotted in the calibration curves. An LOD of 5 ng (Table 3), with a corresponding linear dynamic range of 0.006−1.5 μg, for an electric field of 316 V/cm was obtained, compared with an LOD = 30 ng and dynamic range of 0.06−1.5 μg obtained for FAPA DTIMS with BNG.[34] Increasing the electric field to 476 V/cm improves both LOD and linear dynamic range to 4 ng and 0.006−3 μg, respectively.

**3.9. Gate Depletion Effect.** In this section, the GDE was investigated for BNG and FSG FAPA-DTIMS. First, the original BNG DTIMS configuration was tested. Second, a modified FSG DTIMS configuration was implemented where the DTIMS tube (drift region) was extended 20 mm to accommodate an additional BNG gate (20 mm from the DTIMS inlet aperture), which allowed FSG gating with an inactive BNG (gate is always open) or BNG gating (BNG switches between on and off status). In the case of inactive BNG field switching repeller, the BNG was still present in the IMS cell in order to consider the effect of the physical barrier of BNG wires on the obtained signal intensities (which would obscure the effect of GDE).

As Figure 6 shows, the GDE was investigated for two analytes, acetophenone and pentanone, by plotting the obtained total peak areas as a function of the voltage difference between the BNG wires. In this experiment, the electric field and BNG injection time were 476 V/cm and 300 μs, respectively. According to Figure 6, as the voltage increases, the total peak areas for acetophenone and pentanone decline so that increasing the voltage from 134 to 200 and 140 to 190 V results in a 2.2- and 1.79-fold decrease in the total peak areas, respectively. Increasing the voltage among the wires expands the depletion region that exists on both sides of the BNG, leading to ion loss. Figures S.18 and S.19 demonstrate the GDE on each analyte peak in more detail. As shown in Figure S.18, for acetophenone, reducing the voltage from 200 to 134 V improves the peak area ratio of $S_1/S'_1$ 1.44-fold, while larger increases of 2.55 and 3.49 times are calculated for $S_2/S'_2$ and $S_3/S'_3$, respectively. ($S_1$, $S_2$, $S_3$ are the peak areas above the dashed line for the first, second, and third peak when the BNG voltage is 134 V. $S'_1$, $S'_2$, $S'_3$ are the peak areas above the dashed line for the first, second, and third peak when the BNG voltage is 200 V.) Therefore, as the calculated ratios show, the GDE acts against the ions with higher drift times (lower mobility ions) and reduces the total peak areas more than on ions with shorter drift times. A similar result was observed for pentanone where improvements of 1.52 and 2.69 were calculated for peak area ratios of $S_1/S'_1$ and $S_2/S'_2$ as the voltage among the BNG wires is reduced from 190 to 140 V for the first and second peaks, respectively (Figure S.19).

In the second part of the experiment, the BNG was held in the same position inside the DTIMS cell, and IMS spectra of acetophenone were compared between pulse injections by BNG or repeller separately for two different injection times of 300 and 180 μs. The results are shown in Figures 7 and 8. The calculated peak areas for each peak at two different injection


https://doi.org/10.1021/jasms.1c00309
J. Am. Soc. Mass Spectrom. XXXX, XXX, XXX−XXX

times are shown in Table 4. The total peak area ratio in Figure 7 for the $S_1$ and $S_2$ peaks are improved to 5- and 18-fold, respectively, when the repeller is pulsed instead of the BNG. It is quite clear that in this geometry the discriminatory effect of the depletion region when the BNG is active has a large influence on the lower mobility ions. Since the GDE becomes more important when pulse injection times are lowered, the total peak area ratios of acetophenone's peaks were calculated by lowering the injection time to 180 $\mu$s and shown in Figure 8. In this case, the total peak area is improved 10 times for the first peak and 44 times for the second peak, which corroborates the theory that lower mobility ions suffer more from the GDE effect. In short, using the pulsed repeller instead of the BNG gate not only improves the total ion current that reaches the detector but also enhances the low mobility ion populations, which are necessary in hand-held DTIMS devices in order to achieve high resolutions.

## 4. CONCLUSIONS

In this work, a field-switching repeller technique was used coupled to a FAPA source in a DTIMS and compared with a typical BNG configuration which suffers from GDE. For the generation of discrete packets of ions, a high voltage pulse switched between 5 and 10 kV was applied to the repeller to accelerate the ions into the separation region. The system initially suffered from flow penetration that produced undesired tails in the spectra. In order to remove the large tails, three apertures with different sizes were deployed to optimize the FAPA plasma gas and drift gas linear velocities and control the number of neutral molecules that diffuse into the separation region as well as the ion-neutral molecule reactions inside the separation region. Several repeller and FAPA experimental operating conditions were optimized. Qualitative analysis of a selected set of compounds with a wide range mobilities was also shown. In terms of quantitative analysis, the improved LODs of 5 and 4 ng were obtained for acetaminophen under working electric fields of 316 and 476 V/cm, respectively, when compared with 30 ng obtained in a previous work using a BNG.[34] Also, for 2,6-DTBP, a LOD of 3 ppb was obtained, which is six times lower than previously obtained.[34] The consequences of the GDE were proven for acetophenone and pentanone by changing the voltages applied to the BNG wires. A comparison between acetophenone IMS spectra (under two different pulse injection times of 180 and 300 $\mu$s) was obtained for the BNG and pulsing repeller. The BNG is shown to favor higher mobility ions impacting the overall signal and possibly affect the quantitative analysis of the analytes. This effect seems to be much less pronounced in the case of the pulsing repeller, in particular, at smaller pulsing times. The signal of the lower mobility ions was shown to improve by 5 and 18 times with a 300 $\mu$s pulse and by 10 and 44 times when using a 180 $\mu$s pulse.

## ■ ASSOCIATED CONTENT

### Supporting Information

The Supporting Information is available free of charge at https://pubs.acs.org/doi/10.1021/jasms.1c00309.

RIP spectrum in two different drift gases: helium and nitrogen, the simulation of plasma gas flow trajectories inside the IMS cell without aperture, schematic of ionization region with an aperture (2.5−5 mm) attached to the DTIMS inlet, the simulation of plasma gas flow trajectories with a 2.5 × 5 mm aperture, simulation of drift gas flow in a random plane inside the IMS cell, simulation of the potential field lines inside the IMS cell with SIMION 8.1., RIP spectrum obtained in electric fields of 570 and 620 V/cm, the effect of plasma gas flow rate on the obtained fwhm for single peak of 2,6-DTBP, effect of plasma gas flow rate on the peak intensity of glycerol in different drift gas flow rates, the effect of repeller distance from IMS inlet on the peak intensity and fwhm of 2,6-DTBP, effect of repeller's voltage on the peak intensity of 2,6-DTBP, the effect of FAPA orientation relative to the IMS axis on the 2,6-DTBP peak intensity, the effect of FAPA plasma current on the peak intensities of 2,6-DTBP, calibration curve for 2,6-DTBP under electric field of 316 V/cm, calibration curve of 2,6-DTBP under the electric field of 476 V/cm, mass calibration curve of acetaminophen in electric fields of 316 and 476 V/cm, and the gate depletion effect on the obtained peak area ratios for acetophenone and pentanone in two different BNG voltages of 134 and 200 V (PDF)

## ■ AUTHOR INFORMATION


### Corresponding Authors

**Gerardo Gamez** − *Department of Chemistry and Biochemistry, Texas Tech University, Lubbock, Texas 79409-1061, United States;* orcid.org/0000-0002-8827-6647; Email: gerardo.gamez@ttu.edu

**Carlos Larriba-Andaluz** − *Department of Mechanical and Energy Engineering, Indiana University−Purdue University Indianapolis, Indianapolis, Indiana 46202, United States;* orcid.org/0000-0003-0864-7733; Email: clarriba@iupui.edu

### Authors

**Mohsen Latif** − *Department of Mechanical and Energy Engineering, Indiana University−Purdue University Indianapolis, Indianapolis, Indiana 46202, United States; Mechanical Engineering, Purdue University, West Lafayette, Indiana 47907, United States*

**Xi Chen** − *Department of Mechanical and Energy Engineering, Indiana University−Purdue University Indianapolis, Indianapolis, Indiana 46202, United States; Mechanical Engineering, Purdue University, West Lafayette, Indiana 47907, United States*

**Viraj D. Gandhi** − *Department of Mechanical and Energy Engineering, Indiana University−Purdue University Indianapolis, Indianapolis, Indiana 46202, United States; Mechanical Engineering, Purdue University, West Lafayette, Indiana 47907, United States*

Complete contact information is available at: https://pubs.acs.org/10.1021/jasms.1c00309


### Author Contributions

**CRediT Author Statement: Mohsen Latif:** Methodology, Investigation, Formal analysis, Validation, Visualization, Writing − Original Draft, Writing − Review & Editing. **Xi Chen:** Software (computer modeling), Investigation (computer modeling), Formal analysis (computer modeling), Visualization (computer modeling). **Viraj D. Gandhi:** Software (computer modeling), Investigation (computer modeling), Formal analysis (computer modeling), Visual-

ization (computer modeling). **Carlos Larriba-Andaluz:** Software (computer modeling), Methodology (computer modeling), Validation (computer modeling), Writing – Original Draft, Writing – Review & Editing, Supervision (computer modeling), Project Administration (computer modeling), Funding acquisition (computer modeling). **Gerardo Gamez:** Conceptualization (instrument development), Methodology (instrument development), Validation (instrument development), Visualization (instrument development), Resources (instrument development), Writing – Original Draft, Writing – Review & Editing, Supervision (instrument development), Project Administration (instrument development), Funding acquisition (instrument development).

### Notes

The authors declare no competing financial interest.

## ■ ACKNOWLEDGMENTS

G.G. and M.L. acknowledge funding from Texas Tech University for the work performed on design and construction of the field-switch repeller FAPA DTIMS instrument, as well as all its optimization and performance characterization. G.G. and M.L. thank S. Hiemstra and C. Pfeiffer at the TTU Department of Chemistry and Biochemistry Machine Shop for technical support. C.L.-A. acknowledges funding from Kanomax Holdings as well as Grant No. 2105929 from the Division of Chemical, Bioengineering, Environmental and Transport Systems (Program Director William Olbricht).

## ■ REFERENCES

(1) Eiceman, G.A.; Karpas, Z.; Hill, H. H. Ion mobility spectrometry. In *Ion Mobility Spectrometry*, 3rd ed.; Routledge, 2014; pp 1–400.

(2) Makinen, M. A.; Anttalainen, O. A.; Sillanpää, M. Ion mobility spectrometry and its applications in detection of chemical warfare agents. *Anal. Chem.* **2010**, *82* (23), 9594–9600.

(3) Puton, J.; Namieśnik, J. Ion mobility spectrometry: Current status and application for chemical warfare agents detection. *Trends. Anal. Chem.* **2016**, *85*, 10–20.

(4) Márquez-Sillero, I.; Aguilera-Herrador, E.; Cárdenas, S.; Valcárcel, M. Ion-mobility spectrometry for environmental analysis. *Trends. Anal. Chem.* **2011**, *30* (5), 677–690.

(5) Keller, T.; Miki, A.; Regenscheit, P.; Dirnhofer, R.; Schneider, A.; Tsuchihashi, H. Detection of designer drugs in human hair by ion mobility spectrometry. *Forensic. Sci. Int.* **1998**, *94* (1–2), 55–63.

(6) Sorribes-Soriano, A.; Esteve-Turrillas, F. A.; Armenta, S.; de la Guardia, M.; Herrero-Martínez, J. M. Cocaine abuse determination by ion mobility spectrometry using molecular imprinting. *J. Chromatogr. A* **2017**, *1481*, 23–30.

(7) Coots, J.; Gandhi, V.; Onakoya, T.; Chen, X.; Larriba-Andaluz, C. A parallelized tool to calculate the electrical mobility of charged aerosol nanoparticles and ions in the gas phase. *J. Aerosol Sci.* **2020**, *147*, 105570.

(8) Chen, X.; Gandhi, V.; Coots, J.; Fan, Y.; Xu, L.; Fukushima, N.; Larriba-Andaluz, C. High resolution varying field drift tube ion mobility spectrometer with diffusion autocorrection. *J. Aerosol Sci.* **2020**, *140*, 105485.

(9) Chen, X.; Raab, S. A.; Poe, T.; Clemmer, D. E.; Larriba-Andaluz, C. Determination of gas-phase ion structures of locally polar homopolymers through high-resolution ion mobility spectrometry–mass spectrometry. *J. Am. Soc. Mass Spectrom.* **2019**, *30* (6), 905–918.

(10) Chang, C.-H.; Yeung, D.; Spicer, V.; Ogata, K.; Krokhin, O.; Ishihama, Y. Sequence-Specific Model for Predicting Peptide Collision Cross Section Values in Proteomic Ion Mobility Spectrometry. *J. Proteome Res.* **2021**, *20* (7), 3600–3610.

(11) Burnum-Johnson, K. E.; Zheng, X.; Dodds, J. N.; Ash, J.; Fourches, D.; Nicora, C. D.; Wendler, J. P.; Metz, T. O.; Waters, K. M.; Jansson, J. K. Ion mobility spectrometry and the omics: Distinguishing isomers, molecular classes and contaminant ions in complex samples. *Trends. Anal. Chem.* **2019**, *116*, 292–299.

(12) Wu, T.; Derrick, J.; Nahin, M.; Chen, X.; Larriba-Andaluz, C. Optimization of long range potential interaction parameters in ion mobility spectrometry. *J. Chem. Phys.* **2018**, *148* (7), 074102.

(13) Chen, X.; Raab, S. A.; Poe, T.; Clemmer, D. E.; Larriba-Andaluz, C. Determination of gas-phase ion structures of locally polar homopolymers through high-resolution ion mobility spectrometry–mass spectrometry. *J. Am. Soc. Mass Spectrom.* **2019**, *30* (6), 905–918.

(14) Chen, C.; Tabrizchi, M.; Li, H. Ion gating in ion mobility spectrometry: Principles and advances. *Trends. Anal. Chem.* **2020**, *133*, 116100.

(15) Zhou, L.; Collins, D. C.; Lee, E. D.; Lee, M. L. Mechanical ion gate for electrospray-ionization ion-mobility spectrometry. *Anal. Bioanal. Chem.* **2007**, *388* (1), 189–194.

(16) Clowers, B. H.; Siems, W. F.; Hill, H. H.; Massick, S. M. Hadamard transform ion mobility spectrometry. *Anal. Chem.* **2006**, *78* (1), 44–51.

(17) Li, H.; Giles, K.; Bendiak, B.; Kaplan, K.; Siems, W. F.; Hill, H. H. Resolving structural isomers of monosaccharide methyl glycosides using drift tube and traveling wave ion mobility mass spectrometry. *Anal. Chem.* **2012**, *84* (7), 3231–3239.

(18) Du, Y.; Wang, W.; Li, H. Resolution enhancement of ion mobility spectrometry by improving the three-zone properties of the Bradbury-Nielsen gate. *Anal. Chem.* **2012**, *84* (3), 1725–1731.

(19) Kwasnik, M.; Caramore, J.; Fernández, F. M. Digitally-multiplexed nanoelectrospray ionization atmospheric pressure drift tube ion mobility spectrometry. *Anal. Chem.* **2009**, *81* (4), 1587–1594.

(20) Kai, N.; Jingran, G.; Guangli, O.; Yu, L.; Quan, Y.; Xiang, Q.; Xiaohao, W. A simple template-based transfer method to fabricate Bradbury–Nielsen gates with uniform tension for ion mobility spectrometry. *Rev. Sci. Instrum.* **2014**, *85* (8), 085107.

(21) Zuleta, I. A.; Barbula, G. K.; Robbins, M. D.; Yoon, O. K.; Zare, R. N. Micromachined Bradbury– Nielsen Gates. *Anal. Chem.* **2007**, *79* (23), 9160–9165.

(22) Tabrizchi, M.; Shamlouei, H. Relative transmission of different ions through shutter grid. *Int. J. Mass Spectrom.* **2010**, *291* (1–2), 67–72.

(23) Kirk, A. T.; Zimmermann, S. Bradbury-Nielsen vs. Field switching shutters for high resolution drift tube ion mobility spectrometers. *Int. J. Ion Mobil. Spectrom* **2014**, *17* (3–4), 131–137.

(24) Liu, W.; Davis, A. L.; Siems, W. F.; Yin, D.; Clowers, B. H.; Hill, H. H. Ambient pressure inverse ion mobility spectrometry coupled to mass spectrometry. *Anal. Chem.* **2017**, *89* (5), 2800–2806.

(25) Jenkins, A. US Patent 5:200,614, 1993.

(26) Leonhardt, J. W.; Rohrbeck, W.; Bensch, H. A high resolution IMS for environmental studies. *Int. J. Ion Mobility Spectrom* **2000**, *1*, 43–49.

(27) Kirk, A. T.; Raddatz, C.-R.; Zimmermann, S. Separation of isotopologues in ultra-high-resolution ion mobility spectrometry. *Anal. Chem.* **2017**, *89*, 1509–1515.

(28) Reinecke, T.; Kirk, A. T.; Heptner, A.; Niebuhr, D.; Bottger, S.; Zimmermann, S. A compact high-resolution X-ray ion mobility spectrometer. *Rev. Sci. Instrum.* **2016**, *87*, 053120.

(29) Bunert, E.; Reinecke, T.; Kirk, A. T.; Bohnhorst, A.; Zimmermann, S. Ion mobility spectrometer with orthogonal X-ray source for increased sensitivity. *Talanta* **2018**, *185*, 537–541.

(30) Deng, W.; Gomez, A. Full transient response of Taylor cones to a step change in electric field. *Microfluid. Nanofluid* **2012**, *12* (1–4), 383–393.

(31) Garoz, D.; Bueno, C.; Larriba, C.; Castro, S.; Romero-Sanz, I.; Fernandez de La Mora, J.; Yoshida, Y.; Saito, G. Taylor cones of ionic liquids from capillary tubes as sources of pure ions: The role of surface tension and electrical conductivity. *J. Appl. Phys.* **2007**, *102* (6), 064913.

(32) Kirk, A. T.; Grube, D.; Kobelt, T.; Wendt, C.; Zimmermann, S. High-resolution high kinetic energy ion mobility spectrometer based

on a low-discrimination tristate ion shutter. *Anal. Chem.* **2018**, *90* (9), 5603−5611.

(33) Chen, C.; Tabrizchi, M.; Wang, W.; Li, H. Field Switching Combined with Bradbury−Nielsen Gate for Ion Mobility Spectrometry. *Anal. Chem.* **2015**, *87* (15), 7925−7930.

(34) Latif, M.; Zhang, D.; Gamez, G. Flowing atmospheric-pressure afterglow drift tube ion mobility spectrometry. *Anal. Chim. Acta* **2021**, *1163*, 338507.

(35) Keelor, J. D.; Dwivedi, P.; Fernandez, F. M. An effective approach for coupling direct analysis in real time with atmospheric pressure drift tube ion mobility spectrometry. *J. Am. Soc. Mass Spectrom.* **2014**, *25* (9), 1538−1548.

(36) Cohen, M. J.; Karasek, F. Plasma chromatography—a new dimension for gas chromatography and mass spectrometry. *J. Chromatogr. Sci.* **1970**, *8* (6), 330−337.

(37) Matz, L. M.; Hill, H. H.; Beegle, L. W.; Kanik, I. Investigation of drift gas selectivity in high resolution ion mobility spectrometry with mass spectrometry detection. *J. Am. Soc. Mass Spectrom.* **2002**, *13* (4), 300−307.

(38) Pfeuffer, K. P.; Ray, S. J.; Hieftje, G. Measurement and visualization of mass transport for the flowing atmospheric pressure afterglow (FAPA) ambient mass-spectrometry source. *J. Am. Soc. Mass Spectrom.* **2014**, *25* (5), 800−808.

(39) Tabrizchi, M.; Abedi, A. A novel electron source for negative ion mobility spectrometry. *Int. J. Mass Spectrom.* **2002**, *218* (1), 75−85.

(40) Eiceman, G. A.; Nazarov, E. G.; Rodriguez, J. E.; Bergloff, J. F. Positive reactant ion chemistry for analytical, high temperature ion mobility spectrometry (IMS): Effects of electric field of the drift tube and moisture, temperature, and flow of the drift gas. *Int. J. Ion Mobil. Spectrom* **1998**, *1*, 28−37.

(41) Jafari, M. T. Low-temperature plasma ionization ion mobility spectrometry. *Anal. Chem.* **2011**, *83* (3), 797−803.

(42) Shelley, J. T.; Wiley, J. S.; Chan, G. C.; Schilling, G. D.; Ray, S. J.; Hieftje, G. M. Characterization of direct-current atmospheric-pressure discharges useful for ambient desorption/ionization mass spectrometry. *J. Am. Soc. Mass Spectrom.* **2009**, *20* (5), 837−844.

(43) Viitanen, A.K.; Mauriala, T.; Mattila, T.; Adamov, A.; Pedersen, C.H.; Makela, J.M.; Marjamaki, M.; Sysoev, A.; Keskinen, J.; Kotiaho, T. Adjusting mobility scales of ion mobility spectrometers using 2, 6-DtBP as a reference compound. *Talanta* **2008**, *76* (5), 1218−1223.

(44) Eiceman, G.; Nazarov, E. G.; Stone, J. A. Chemical standards in ion mobility spectrometry. *Anal. Chim. Acta* **2003**, *493* (2), 185−194.

(45) Leasure, C.; Fleischer, M.; Anderson, G.; Eiceman, G. Photoionization in air with ion mobility spectrometry using a hydrogen discharge lamp. *Anal. Chem.* **1986**, *58* (11), 2142−2147.

(46) Rudnicka, J.; Mochalski, P.; Agapiou, A.; Statheropoulos, M.; Amann, A.; Buszewski, B. Application of ion mobility spectrometry for the detection of human urine. *Anal. Bioanal. Chem.* **2010**, *398* (5), 2031−2038.

(47) Borsdorf, H.; Fiedler, P.; Mayer, T. The effect of humidity on gas sensing with ion mobility spectrometry, Sens. Actuators B Chem. *Sensors and Actuators B: Chemical* **2015**, *218*, 184−190.



https://doi.org/10.1021/jasms.1c00309
*J. Am. Soc. Mass Spectrom.* XXXX, XXX, XXX−XXX